PHYSICAL REVIEW B **79**, 054524 (2009)

Superconductivity in lithium under high pressure investigated with density functional and Eliashberg theory

Yansun Yao,[1,2] J. S. Tse,[1,*] K. Tanaka,[1,†] F. Marsiglio,[3] and Y. Ma[4]

[1]*Department of Physics and Engineering Physics, University of Saskatchewan, 116 Science Place, Saskatoon, Saskatchewan, Canada S7N 5E2*

[2]*Steacie Institute for Molecular Sciences, National Research Council of Canada, Ottawa, Ontario, Canada K1A 0R6*

[3]*Department of Physics, University of Alberta, 11322-89 Avenue, Edmonton, Alberta, Canada T6G 2G7*

[4]*National Laboratory of Superhard Materials, Jilin University, Changchun 130012, People's Republic of China*

(Received 16 December 2008; revised manuscript received 18 January 2009; published 24 February 2009)

Structural phase transitions and superconducting properties in three phases (9*R*, fcc, and *cI*16) of solid Li are investigated using a pseudopotential plane-wave method based on density functional perturbation theory. In particular, it is shown that phonon softening is responsible for a pressure-induced fcc→*cI*16 transition as well as for a significant enhancement of electron-phonon coupling and superconducting transition temperature T_c preceding this structural transformation. The nature of superconductivity in the fcc and *cI*16 phases is examined by solving the Eliashberg equations with the spectral function $\alpha^2F(\omega)$ obtained from first-principles calculations and by evaluating the functional derivative $\delta T_c/\delta\alpha^2F(\omega)$. The calculated T_c reaches a maximum at pressure close to the fcc→*cI*16 transition and is significantly reduced in the *cI*16 phase, in agreement with the trend observed experimentally. The variation in T_c as a function of pressure is explained in terms of the functional derivative and shifts of the spectral weight.

DOI: 10.1103/PhysRevB.79.054524 PACS number(s): 71.15.−m, 71.20.Dg, 74.20.−z, 74.62.Fj

I. INTRODUCTION

Under ambient conditions, Li crystallizes in the body-centered-cubic (bcc) structure. Although bcc Li is often considered as a "simple" metal, electronic structure calculation has revealed a strong participation of weakly degenerate 2*p* orbitals in the chemical bonding already at ambient pressure.[1] Upon cooling, bcc Li goes through a martensitic transition to 9*R* Li (*R*-3*c*) at around 75 K.[2–5] Upon compression, bcc Li transforms successively from bcc→face centered cubic (fcc)→*hR*1(SG *R*-3*c*)→*cI*16 (SG *I*-43*d* or *Ia*-3*d*).[6–9] There is evidence found in ac susceptibility and Raman spectroscopic measurements that *cI*16 Li further transforms into a new phase at around 50 GPa and stabilizes into another high-pressure polymorph above 62 GPa.[10] Recent theoretical studies, however, predict that *cI*16 Li is stable up to pressure higher than 88 GPa and then transforms to an orthorhombic structure (*Cmca*-24 Li).[11] Significantly, it has been observed that Li is superconducting for pressures from 20 to 80 GPa.[12–15] The pressure dependence of the superconducting transition temperature T_c suggests that there may be three distinct superconducting phases within this pressure range. Moreover, theoretical studies predicted superconductivity in Li also under ambient pressure.[16–22] For a long time, however, this prediction was not verified.[23,24] This puzzle has finally been resolved recently by a susceptibility measurement showing that solid Li at ambient pressure is weakly superconducting with $T_c \leq 0.4$ mK.[25]

The temperature- and pressure-induced phase transitions and superconductivity in high-pressure Li have been investigated experimentally. Theoretical works on pressure-induced superconductivity so far, however, have focused on the fcc phase only.[26–37] The only exception is the study on fcc and *cI*16 by Christensen and Novikov[26] based on a rigid muffin-tin approximation—which proved to be inadequate for Li (Ref. 34)—and without calculation of the phonon spectra for *cI*16. The predicted T_c was much too high for fcc as well as *cI*16 even by introducing an additional term modeling spin fluctuations in the McMillan equation.[26] In the present work, the pressure-induced fcc→*cI*16 transition and superconductivity near this transition and in the *cI*16 phase are investigated by means of first-principles calculation. The phonon spectra and the electron-phonon spectral function $\alpha^2F(\omega)$ are calculated by linear response theory and density functional perturbation theory (DFPT). The T_c is evaluated by solving the Eliashberg equations directly and numerically. The effectiveness of phonons in various frequency regions in raising T_c is also studied in terms of the functional derivative $\delta T_c/\delta\alpha^2F(\omega)$. It is found that Li undergoes the fcc→*cI*16 phase transition at around 33 GPa, and for pressure close to the transition point, substantial phonon softening occurs. A drastic variation in T_c across the fcc→*cI*16 transition, consistent with the observed trend,[14,15] is found and explained in terms of shifts of the spectral weight. For completeness, we also revisit the 9*R*→bcc phase transition and examine its mechanism and the superconducting behavior at ambient pressure.

The paper is organized as follows. In Sec. II computational details are described. The 9*R* and bcc phases at ambient pressure are discussed in Sec. III A, the fcc→*cI*16 transition in Sec. III B, and superconductivity in the *cI*16 phase in Sec. III C. The work is summarized in Sec. IV.

II. COMPUTATIONAL DETAILS

The electron-phonon interaction is investigated by means of the Eliashberg theory,[38] with the spectral function obtained by first-principles calculation. The electron-phonon coupling (EPC) parameter λ is evaluated by a weighted av-

erage over the mode EPC parameters λ_{qj} for all phonon modes (qj) of a complete q-point mesh in the first Brillouin zone (BZ),

$$\lambda = \sum_{qj} \lambda_{qj} w(q), \tag{1}$$

where $w(q)$ is the weight of phonon mode (qj). For each mode j and wave vector q, λ_{qj} is calculated by linear response theory and DFPT (Refs. 39 and 40) using the program package QUANTUM-ESPRESSO.[41] The electron-phonon spectral function, $\alpha^2F(\omega)$, is defined in terms of the phonon linewidth γ_{qj} of mode (qj) as

$$\alpha^2F(\omega) = \frac{1}{2\pi N(\epsilon_F)} \sum_{qj} \frac{\gamma_{qj}}{\omega_{qj}} \delta(\omega - \omega_{qj}) w(q), \tag{2}$$

where ω_{qj} is the mode frequency and $N(\epsilon_F)$ is the density of states (DOS) at the Fermi level ϵ_F. The γ_{qj} is given by

$$\gamma_{qj} = 2\pi\omega_{qj} \sum_{nm} \int \frac{d^3k}{\Omega_{\mathrm{BZ}}} |g^j_{kn,k+qm}|^2 \delta(\epsilon_{kn} - \epsilon_F) \delta(\epsilon_{k+qm} - \epsilon_F), \tag{3}$$

where the integral is taken over the first BZ, with Ω_{BZ} as the volume of the BZ. The ϵ_{kn} and ϵ_{k+qm} are the Kohn-Sham eigenvalues with wave vectors k and $k+q$ in the nth and mth bands, respectively. The electron-phonon matrix elements, $g^j_{kn,k+qm}$, are determined from the linearized self-consistent potential. The γ_{qj} is related to the mode EPC parameter λ_{qj} by

$$\lambda_{qj} = \frac{\gamma_{qj}}{\pi\hbar N(\epsilon_F)\omega^2_{qj}}. \tag{4}$$

The EPC parameter λ can also be given in terms of the spectral function by

$$\lambda = 2\int \frac{\alpha^2F(\omega)}{\omega} d\omega. \tag{5}$$

The Eliashberg equations[38,42] are solved numerically to find the superconducting transition temperature T_c. On the imaginary frequency axis, they consist of coupled nonlinear equations for the frequency-dependent order parameter $\Delta(i\omega_n)$ and renormalization factor $Z(i\omega_n)$ at the Matsubara frequencies,

$$\Delta(i\omega_n)Z(i\omega_n) = \pi T \sum_{m=-\infty}^{\infty} [\lambda(i\omega_m - i\omega_n) - \mu^*(\omega_c)\Theta(\omega_c - |\omega_m|)] \frac{\Delta(i\omega_m)}{\sqrt{\omega_m^2 + \Delta^2(i\omega_m)}} \tag{6}$$

and

$$Z(i\omega_n) = 1 + \frac{\pi T}{\omega_n} \sum_m \lambda(i\omega_m - i\omega_n) \frac{\omega_m}{\sqrt{\omega_m^2 + \Delta^2(i\omega_m)}}, \tag{7}$$

where $\omega_n = \pi T(2n-1)(n=0, \pm 1, \pm 2, \ldots)$ with T as the temperature and $\Theta(\omega_c - |\omega_m|)$ is the Heaviside step function. The cutoff frequency ω_c is taken to be some multiple (typically six) of the maximum phonon frequency and $\mu^*(\omega_c)$ is the Coulomb pseudopotential scaled to the cutoff frequency. The $\lambda(i\omega_m - i\omega_n)$ is determined from the spectral function by

$$\lambda(i\omega_m - i\omega_n) = 2\int_0^\infty d\omega \frac{\omega\alpha^2F(\omega)}{\omega^2 + (\omega_n - \omega_m)^2}. \tag{8}$$

Defining $\tilde{\omega}_n \equiv \omega_n Z(i\omega_n)$ and $\tilde{\Delta}(i\omega_n) \equiv \Delta(i\omega_n)\tilde{\omega}_n/\omega_n$, Eqs. (6) and (7) become

$$\tilde{\Delta}(i\omega_n) = \pi T \sum_m [\lambda(i\omega_m - i\omega_n) - \mu^*(\omega_c)\Theta(\omega_c - |\omega_m|)] \frac{\tilde{\Delta}(i\omega_m)}{\sqrt{\tilde{\omega}_m^2 + \tilde{\Delta}^2(i\omega_m)}} \tag{9}$$

and

$$\tilde{\omega}_n = \omega_n + \pi T \sum_m \lambda(i\omega_m - i\omega_n) \frac{\tilde{\omega}_m}{\sqrt{\tilde{\omega}_m^2 + \Delta^2(i\omega_m)}}. \tag{10}$$

In the limit $T \to T_c$, these equations are linearized and a pair-breaking parameter ρ (Refs. 43 and 44) is introduced,

$$\sqrt{\tilde{\omega}_m^2 + \Delta^2(i\omega_m)} \approx |\tilde{\omega}_m| + \rho \quad \rho \to 0, \tag{11}$$

so that one has an eigenvalue equation,

$$\rho\bar{\Delta}_n = \pi T_c \sum_m \left[\lambda(i\omega_m - i\omega_n) - \mu^*(\omega_c)\Theta(\omega_c - |\omega_m|) - \delta_{m,n} \frac{|\tilde{\omega}_n|}{\pi T_c} \right] \bar{\Delta}_m \equiv \sum_m K_{nm}\bar{\Delta}_m, \tag{12}$$

where $\bar{\Delta}_n \equiv \tilde{\Delta}(i\omega_n)/(|\tilde{\omega}_n| + \rho)$. The matrix K_{nm} is diagonalized for each T and T_c is obtained as T for which the largest eigenvalue $\rho = 0$.

One can examine the contributions from phonons in various frequency regions to T_c in terms of the functional derivative with respect to the spectral function defined by[43]

$$\Delta T_c = \int_0^\infty d\omega \frac{\delta T_c}{\delta\alpha^2F(\omega)} \Delta\alpha^2F(\omega). \tag{13}$$

It is given by

$$\frac{\delta T_c}{\delta\alpha^2F(\omega)} = -\frac{\bar{\delta}\rho}{\bar{\delta}\alpha^2F(\omega)} \Big/ \left[\frac{\partial\rho}{\partial T}\right]_{T_c}, \tag{14}$$

where the numerator on right-hand side implies variation in ρ with respect to $\alpha^2F(\omega)$ only through the explicit dependence of K_{nm} on $\alpha^2F(\omega)$.

Another property of considerable interest is the energy gap, which appears in the superconducting state as the order parameter becomes nonzero. An efficient calculation of this quantity proceeds in two steps. First the order parameter on the imaginary axis is solved by iterating Eqs. (9) and (10) to convergence. Then a hybrid set of equations is converged to solve for the order parameter $\Delta(\omega + i\delta)$ [and the renormalization function, $Z(\omega + i\delta)$] on the real axis (δ here is a real and positive number and $\delta \to 0$).[45] The (zero-temperature) energy

gap is then defined by the point at which the quasiparticle density of states,

$$\frac{N(\omega)}{N(0)} = \mathrm{Re}\frac{\omega}{\sqrt{\omega^2 - \Delta^2(\omega + i\delta)}}, \tag{15}$$

becomes nonzero. This occurs when $\omega = \mathrm{Re}\,\Delta(\omega + i\delta)$; the frequency that satisfies this equation is identified as the energy gap, Δ_0. The $N(0)$ above is the Fermi-surface (FS) density of states.

The dimension of the matrix K_{nm} in Eq. (12) is determined by the maximum Matsubara frequency that satisfies $|\omega_n| \leq \omega_c$ and thus becomes significantly large for low temperature. As will be discussed below, T_c for both $9R$ and bcc Li at ambient pressure is very low, and solving Eq. (12) becomes increasingly difficult as the Coulomb pseudopotential μ^* increases. In such a case, one can utilize the approximate McMillan equation[46] with the Allen-Dynes modification[47] to calculate T_c,

$$T_c = \frac{\omega_{\log}}{1.2}\exp\left[-\frac{1.04(1+\lambda)}{\lambda - \mu^*(1+0.62\lambda)}\right], \tag{16}$$

where

$$\omega_{\log} = \exp\left[\frac{2}{\lambda}\int_0^\infty \frac{d\omega}{\omega}\alpha^2 F(\omega)\ln\,\omega\right]. \tag{17}$$

Corresponding to a given $\mu^* = \mu^*(\omega_c)$ in the Eliashberg equation, the choice of the value of μ^* in Eq. (16) is somewhat arbitrary. One choice is to scale μ^* to $\omega_{\log}$, i.e.,

$$\mu^*(\omega_{\log}) \approx \frac{\mu}{1 + \mu\,\ln(\epsilon_F/\omega_{\log})}, \tag{18}$$

where μ is the direct Coulomb repulsion parameter.[48,49]

III. RESULTS

A. Ambient-pressure $9R \rightarrow$bcc transition

At ambient pressure and below 75 K, bcc Li undergoes a martensitic phase transition to a close-packed structure. The low-temperature structure was initially assumed to be hexagonal close packed (hcp) (*ABABAB*) (Ref. 2) but eventually identified to be the samarium-type $9R$ structure[3–5] with a nine-layer stacking sequence *ABCBCACAB*. The superconductivity of Li under ambient pressure has been a subject of many experimental and theoretical investigations. A theoretical analysis using the Eliashberg theory has predicted a T_c close to 1 mK for $9R$ Li (0.1 K for bcc Li), assuming $\mu^* \approx 0.2$ (scaled to the maximum phonon frequency).[20,21] This prediction is consistent with the measured T_c of 0.4 mK.[25] Moreover, this value has correctly been predicted by means of the Eliashberg theory in which electron-electron interactions are treated before electron-phonon coupling is included.[19]

The $9R \rightarrow$bcc transition is an entropy-driven structural transformation. Since the experimentally observed transition temperature (~75 K) is far below the melting point of Li (~454 K) at ambient pressure, anharmonic effects are not expected to play an important role. This transition may then be described within a quasiharmonic approximation by taking into account the static internal energy and the vibrational entropy. The free energy is given by

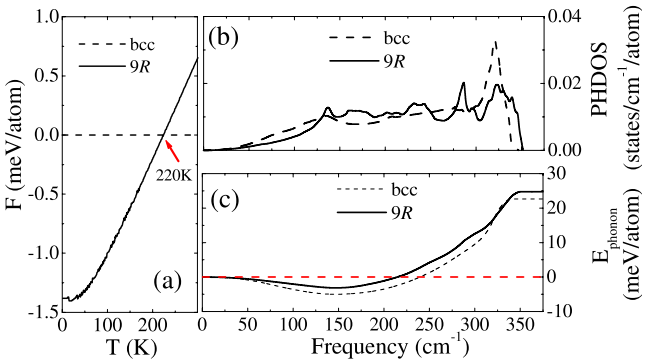

FIG. 1. (Color online) The phase transition from $9R$ to bcc Li estimated with the harmonic approximation at ambient pressure. (a) Calculated free energies of bcc and $9R$ Li as a function of temperature. The free energy of bcc Li is taken as a reference, and the estimated critical temperature is marked. (b) The phonon DOS for bcc and $9R$ Li. (c) The integrated vibrational energy E_{phonon} for bcc and $9R$ Li as a function of vibrational frequency ω calculated at 220 K.

$$F(V,T) = E_0(V) + k_B T\int_0^\infty g(\omega)\ln\left[2\,\sinh\left(\frac{\hbar\omega}{2k_B T}\right)\right]d\omega, \tag{19}$$

where $E_0(V)$ is the static crystal energy, the second term is the vibrational energy E_{phonon}, and $g(\omega)$ is the phonon density of states (PHDOS) at frequency ω.

The equilibrium lattice parameters, the static crystal energy, and the PHDOS of $9R$ and bcc Li have been computed using DFPT with the plane-wave (PW) pseudopotential method.[39–41] All the calculations were performed using the QUANTUM-ESPRESSO package,[41] employing a norm-conserving pseudopotential with local density approximation (LDA). The electronic calculations were performed with $12\times12\times12$ and $16\times16\times16$ MP k meshes[50] for the $9R$ and bcc phases, respectively. For both phases, the PHDOS was obtained from individual phonons calculated on a $8\times8\times8$ MP q mesh using the tetrahedron method.[51]

Figure 1(a) displays the free energy difference between $9R$ and bcc Li as a function of temperature. At $T=0$ K, the $9R$ structure is more stable than bcc by 1.4 meV/atom. The free energy difference decreases as temperature increases and the energetic order is reversed with the bcc phase becoming more stable at ~220 K. The difference in the free energy of $9R$ and bcc Li shown in Fig. 1(a) can be understood by examining the PHDOS in the two phases. As shown in Fig. 1(b), compared to $9R$, the PHDOS of the bcc phase is weighed more heavily in the low-frequency (below 140 cm^{-1}, acoustic branch) region. It can be seen in Eq. (19) that at a given temperature, low-frequency vibrations are more effective in reducing the vibrational energy, E_{phonon}, than high-frequency vibrations are. Thus the difference in the

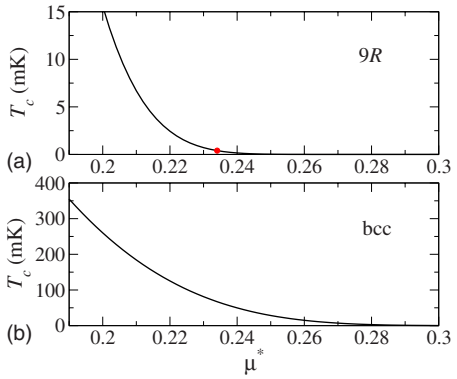

FIG. 2. (Color online) The superconducting transition temperature T_c evaluated from the Allen-Dynes (Ref. 47) modified McMillan equation [Eq. (16)] as a function of μ^* for (a) 9*R* Li and (b) bcc Li at ambient pressure. The observed $T_c \simeq 0.4$ mK (Ref. 25) is marked as a circle.

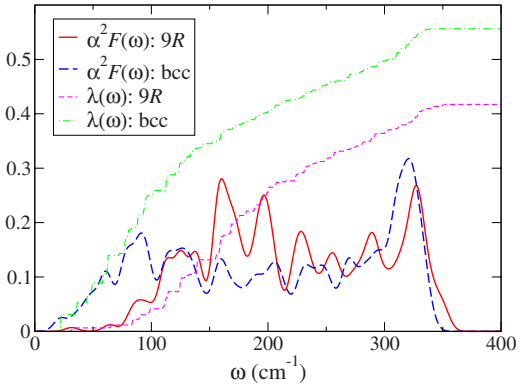

FIG. 3. (Color online) The electron-phonon spectral function $\alpha^2F(\omega)$ and the integrated EPC parameter λ as a function of frequency ω for bcc and 9*R* Li.

PHDOS in the low-frequency region between the 9*R* and bcc phases yields a notable difference in E_{phonon}. To demonstrate this, the integrated vibrational energy of 9*R* and bcc Li calculated at 220 K are plotted as a function of ω in Fig. 1(c). As can be seen in this figure, at low frequencies, integrated vibrational energy drops much faster in bcc than in 9*R*, resulting in a smaller total integrated value over the entire frequency range. At sufficiently high temperature (~220 K in this case) the vibrational energy difference becomes larger than the difference in the static crystal energy (not shown). Consequently the 9*R* phase transforms into the bcc structure. The transformation temperature of ~220 K is consistent with the result of the earlier theoretical study,[20] while it is substantially higher than the experimentally observed transition temperature, 75 K, upon cooling.[2–5] However, since the transformation upon cooling starts with nucleation of the 9*R* phase within the bcc matrix, the observed starting temperature of 75 K represents a lower bound on the transition temperature.[20]

The EPC parameter and the spectral function in the 9*R* and bcc phases have been calculated by Eqs. (1) and (2), respectively. For both structures, the mode EPC parameter λ_{qj} has been calculated in the first BZ on an $8\times8\times8$ MP q-point mesh. Individual λ_{qj} at each wave vector q was evaluated with a $24\times24\times24$ MP k-point mesh for 9*R* Li and a $32\times32\times32$ MP k-point mesh for bcc Li. From Eq. (1) the total EPC parameter λ is found to be 0.41 and 0.52 for 9*R* and bcc, respectively. These λ values are in fair agreement with the previously predicted values of 0.34 for 9*R* and 0.45 for bcc.[20,21] Our λ value for bcc Li is also comparable to 0.4 reported in Ref. 33 but deviates significantly from 0.19 reported in Ref. 32. A possible reason for slightly larger λ in the present study is that the LDA exchange correlation tends to underestimate the equilibrium volume and hence overestimate the overall phonon frequencies. As a result, our superconducting transition temperature T_c discussed below is higher than that found in Refs. 20 and 21.

The T_c for 9*R* and bcc Li evaluated from Eq. (16) is plotted as a function of μ^* in Fig. 2. The $\omega_{\log}$ are 251 K for 9*R* and 161 K for bcc. The T_c for bcc Li is substantially higher than that of 9*R* for a given μ^*, and for bcc one would need an unrealistic value of μ^* to reproduce the experimental value of $T_c \simeq 0.4$ mK.[25] For 9*R* Li, on the other hand, our calculation can reproduce the experimental T_c with $\mu^* \simeq 0.234$ (shown as a red circle in Fig. 2). This relatively large value of μ^* is supported by the estimate ($\mu^* \approx 0.24$) by Richardson and Ashcroft for 9*R* Li,[19] who have found that the effects of the Coulomb repulsion can be significant in this low-density metal and underestimated substantially if the nominal value of $\mu^* \approx 0.1$ is used in the McMillan equation. The fact that 9*R* is more stable than bcc at low temperature and T_c is consistent with the experimental value strongly suggest that 9*R* is indeed the superconducting phase. The substantial difference in T_c between 9*R* and bcc is due to large λ in the latter structure. The spectral function $\alpha^2F(\omega)$, shown in Fig. 3 as a function of ω, has more weight in the low-frequency region in the bcc phase than in the 9*R* phase. Also plotted in Fig. 3 is the integrated EPC parameter $\lambda(\omega)$. Since low-frequency phonons contribute more effectively to EPC, the larger value of $\alpha^2F(\omega)$ at low frequencies results in a rapid rise of $\lambda(\omega)$ for small ω and enhances the total λ in bcc Li.

B. High pressure fcc→*cI*16 transition

In contrast to the nearly free electron behavior under ambient conditions, high-pressure phases of Li are expected to possess very different physical and electronic properties. It has been predicted that a dramatic change in the electronic structure leading to a reduced-symmetry phase with a "paired-atom" structure may occur at very high pressure.[52] This suggestion motivated an x-ray diffraction experiment performed at $T=180$ K.[7] It was observed that bcc Li transforms to an fcc phase at around 7.5 GPa. Further compression leads to a mixture of two structures, *hR*1 and *cI*16, at 39.8 GPa. Initially the *hR*1 structure is the dominant component, while it gradually transforms to *cI*16 with increasing pressure and the *hR*1 component disappears at 42.5 GPa. Approximate electronic structure calculations based on a rigid muffin-tin approximation predicted that fcc Li is superconducting with T_c increasing rapidly with pressure and reaching 50–70 K.[26] Superconductivity was confirmed by subsequent experiments.[13–15] However, in all these experi-

ments the observed T_c was much lower than predicted by the work in Ref. 26. The T_c was found to be strongly pressure dependent,[13–15] but the detailed behavior is not consistent among these different experiments.

In the experiment in Ref. 15, ac susceptibility and electrical resistivity measurements up to 67 GPa in a nearly hydrostatic environment were performed. The T_c determined by this experiment is expected to be more precise compared to the earlier experiments,[13,14] and it was found that the onset of the superconducting state is at 20.3 GPa. The T_c increases rapidly as pressure increases from 5.4 to 14 K at 30 GPa. Then it decreases with pressure up to 50 GPa. At pressure higher than 50 GPa, T_c increases again and superconductivity disappears abruptly at 62 GPa. A maximum in T_c has also been observed in the earlier experiment under nonhydrostatic conditions[14] but at a slightly higher pressure of 33 GPa. Changes in T_c reflected in vibrational frequencies in the Raman spectra have also been observed.[10] These changes have been attributed to structural transitions. The peak in T_c at 30 GPa (Ref. 15) is most likely related to the fcc $\rightarrow$ *cI*16/*hR*1 transition. It is possible that at 50 and 62 GPa, two successive phase transitions occur to new unknown structures.[15]

There have been extensive theoretical studies of superconductivity in the fcc phase of Li under pressure.[26,28–37] In particular, it has been suggested that superconductivity in fcc Li is driven by Fermi-surface nesting[30,31] and Kohn anomalies,[30] resulting in an unusually high T_c. On the other hand, no theoretical investigation has been made on superconductivity of the high-pressure *cI*16 phase based on first-principles calculation of the phonon spectra and the electron-phonon spectral function. Furthermore, the observed maximum in T_c close to the fcc $\rightarrow$ *cI*16 phase transition has not been explained. In this work, the phase transition fcc $\rightarrow$ *cI*16 and superconductivity in both of these phases are studied.

The enthalpies of fcc, *hR*1, *cI*16, and *Cmca*-24 Li have been calculated at different pressures with stringent criteria. Total-energy calculations were performed with the program VASP (Ref. 53) using the projected augmented wave (PAW) pseudopotential,[54] with 1*s* and 2*s* as valence states and a plane-wave energy cutoff of 350 eV. The LDA exchange-correlation functional was used. For fcc and *cI*16 Li, a $24\times24\times24$ MP *k*-point mesh was used to sample the first BZ. For *hR*1 and *Cmca*-24 Li, a smaller $16\times16\times16$ MP *k*-point mesh was found to be sufficient. The calculated enthalpies as a function of pressure for the four polymorphs are compared in Fig. 4. Below 46 GPa, the enthalpy difference between *hR*1 and fcc Li is not discernible in the scale shown. The *hR*1 structure has a rhombohedral cell that can be related to a distorted fcc cell with larger cell angles ($\alpha>60°$) increasing with pressure.[7] As shown in Fig. 5, the cell angle of *hR*1 Li increases very gradually at low pressure, indicating minor distortions of the fcc cell ($\alpha=60°$). Therefore, the energy difference between the two phases is small. At pressure higher than 46 GPa, the rhombohedral cell angle increases rapidly and the energy difference between the two phases becomes significant. In the x-ray experiment at $T=180$ K in Ref. 9, the *hR*1 structure was found to coexist with *cI*16 Li in a narrow pressure range near the fcc $\rightarrow$ *cI*16 phase transition. However, our calculation of the phonon band structure of the *hR*1 phase at 33 GPa shows that it is unstable with a very large imaginary frequency; see inset of Fig. 5, where an imaginary frequency (negative eigenvalue) is represented by a negative frequency. This discrepancy between the theory and the experiment suggests the possibility that *hR*1 Li is entropically stabilized only at high temperature and does not exist at low temperature, for which the superconductivity measurements[13–15] were conducted. A piece of evidence supporting this conjecture is that the ac susceptibility measurement at low temperature[15] did not show any notable change in T_c within the pressure range where the fcc/*hR*1/*cI*16 are expected to coexist. Therefore, *hR*1 Li is not considered further in this work. The *cI*16 phase becomes more stable than fcc at around 33 and up to 110 GPa, where *Cmca*-24 Li becomes more stable. The calculated pressure of ~33 GPa for the fcc $\rightarrow$ *cI*16 transition is lower than the transition pressure of 39.8 GPa for fcc $\rightarrow$ *hR*1/*cI*16 observed at $T=180$ K.[7] On the other hand, it is close to 30–33 GPa, at which a distinct feature was observed in the T_c measurements.[14,15] This indicates that the peak in T_c observed in these experiments may be related to a structural change. On the other hand, the transition pressure predicted for *cI*16 $\rightarrow$ *Cmca*-24 at 110 GPa implies that *Cmca*-24 Li is not a viable candidate for the unknown su-

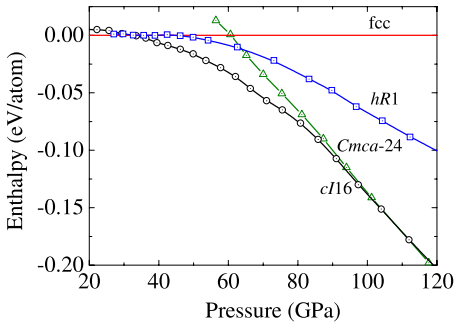

FIG. 4. (Color online) The enthalpies per atom for fcc, *hR*1, *cI*16, and *Cmca*-24 Li as a function of pressure. The enthalpy for fcc Li is taken as a reference. Our calculation indicates that the *cI*16 phase becomes more stable than fcc at roughly 33 GPa. The experimentally observed pressure for the fcc $\rightarrow$ *hR*1/*cI*16 transformation at 180 K is 39.8 GPa.

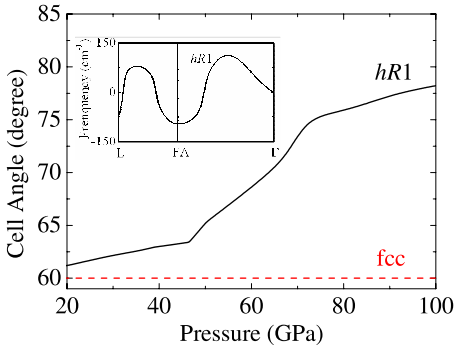

FIG. 5. (Color online) The cell angle for the *hR*1 structure as a function of pressure. The *hR*1 structure is in rhombohedral setting ($\alpha>60°$) and to be compared with fcc cell ($\alpha=60°$). (Inset) The acoustic phonon branch for *hR*1 Li calculated at 33 GPa.

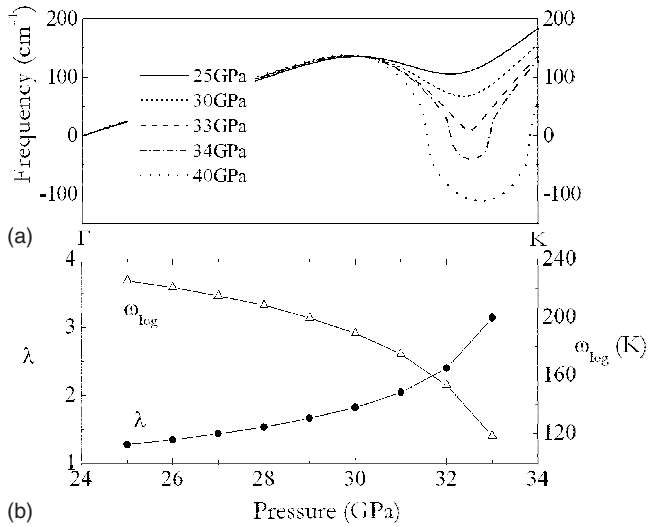

FIG. 6. (a) The evolution of the acoustic phonon branch for fcc Li along the $\Gamma \rightarrow K$ direction within the pressure range of 25–40 GPa. (b) The calculated λ and $\omega_{\log}$ for fcc Li as a function of pressure up to the critical point 33 GPa for the transition to *cI*16 Li.

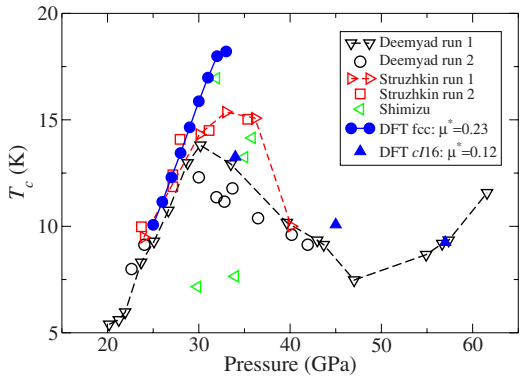

FIG. 7. (Color online) The calculated T_c as a function of pressure for fcc and *cI*16 Li in comparison with the experimental data (Refs. 13–15). The numerical results are represented in solid symbols and lines, and the experimental data in open symbols and dashed lines.

perconducting phase suggested to exist for pressure from 50 to 60 GPa.[11]

The phonon spectra of fcc Li have been obtained by linear response theory.[41] Individual phonons were calculated on an $8\times8\times8$ q-point mesh with a $16\times16\times16$ k-point mesh used for the first BZ integrations. The phonon dispersions of fcc Li have been calculated within the pressure range of 25–40 GPa. In agreement with the previous theoretical studies,[30,31,35,36] a notable feature in the phonon band structure of fcc Li is the gradual development of a soft transverse acoustic (TA) mode along the $\Gamma \rightarrow K$ direction with increasing pressure. The upper panel of Fig. 6(a) shows the phonon dispersion along $\Gamma \rightarrow K$ at selected pressures. The soft mode was found to vanish at about 33 GPa. As pressure is increased slightly to 34 GPa, an imaginary frequency at 50 cm^{-1} appears. The appearance of an imaginary mode indicates that fcc Li is now mechanically unstable. This instability at ~33 GPa is in close proximity to the pressure for the fcc$\rightarrow$*cI*16 transition predicted by the enthalpy calculation described above (Fig. 4). Thus softened phonons are responsible for initiating the structural transition. It has also been found in the earlier studies[30,31] that softened phonons induce strong Fermi-surface nesting and a significant enhancement of the EPC.

One of the objectives of this investigation is to understand the observed maximum in T_c near the fcc$\rightarrow$*cI*16 phase transition. The EPC of fcc Li has been analyzed in the pressure range from 25 to 33 GPa. The mode EPC parameters λ_{qj} have been computed in the first BZ on a $12\times12\times12$ MP q-point mesh. Individual λ_{qj} at each q point was calculated with a $32\times32\times32$ MP k-point mesh. The EPC parameter λ and the logarithmic average of phonon frequencies $\omega_{\log}$ for fcc Li are shown as a function of pressure in the lower panel of Fig. 6. At lower pressure, λ and $\omega_{\log}$ slowly increases and decreases, respectively. However, as pressure approaches 33 GPa, λ increases rapidly, while $\omega_{\log}$ decreases significantly. From 32 to 33 GPa, λ changes from 2.39 to 3.14 with a 31% increase. The $\omega_{\log}$ decreases from 153 to 118 K; it is reduced by about 23%. This large reduction in $\omega_{\log}$ is a consequence of the softening of TA phonons near the K point. At the same time, the EPC parameters λ_{qj} for those modes near the K point are enhanced dramatically due to their inverse proportionality to ω_{qj}, resulting in a notable increase in the total λ. The EPC is thus strongest and $\lambda=3.14$ at 33 GPa.

The superconducting critical temperature T_c has been calculated by solving the Eliashberg equations, i.e., by solving the eigenvalue problem in Eq. (12), and is shown in Fig. 7 along with the experimental data.[13–15] We have used a calculated spectral function $\alpha^2F(\omega)$ appropriate for each pressure, while $\mu^*(\omega_{\log})$ has been chosen to be 0.23 for all pressures. For pressure $\leq$29 GPa, our calculation reproduces the measured T_c, for which the three experimental results are consistent. At higher pressure, T_c reaches a maximum at 33 GPa in agreement with the trend found in the experiment in Ref. 14, while T_c measured in the experiment in Ref. 15 peaks at 30 GPa. The calculated T_c increases monotonically for pressures from 25 to 32 GPa, but its slope as a function of pressure becomes much smaller from 32 to 33 GPa. In view of the substantial phonon softening in fcc Li at pressure close to 33 GPa, it is not unreasonable to attribute the difference between the predicted and observed T_c for pressure 30–33 GPa to the neglect of anharmonic effects. It has been shown theoretically[55] and experimentally[56] that in the "high-temperature" superconductor MgB_2, anharmonicity plays a significant role in reducing T_c.

The phonon softening is reflected in the spectral function $\alpha^2F(\omega)$, and the increase in T_c as a function of pressure from 25 to 33 GPa can be understood in terms of $\alpha^2F(\omega)$ compared with the functional derivative $\delta T_c/\delta\alpha^2F(\omega)$. In Fig. 8, $\delta T_c/\delta\alpha^2F(\omega)$ is presented as a function of frequency ω in the fcc phase for pressure 25–33 GPa. As a function of ω/T_c, the functional derivative is expected to have a universal form that is positive for all frequencies and linear in the low-frequency limit, and peaks at $\omega/T_c\approx2\pi$.[43,57] As can be seen in Fig. 8, $\delta T_c/\delta\alpha^2F(\omega)$ for fcc Li indeed has such a universal form for all pressures, and its overall magnitude decreases monotonically as pressure is increased. In Fig. 9 the spectral function and the functional derivative are plotted together for

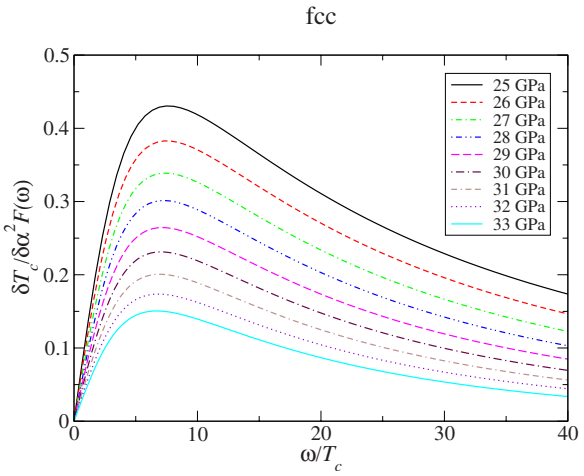

FIG. 8. (Color online) The functional derivative $\delta T_c/\delta\alpha^2F(\omega)$ as a function of frequency ω/T_c for various pressures in the fcc phase.

pressures (a) 25 and (b) 29 GPa. As pressure increases from 25 GPa, the spectral weight, mainly focused on the range $\omega\sim 100-300$ cm^{-1}, shifts toward lower frequencies. In particular, the highest peak in the region $\omega\sim 100-120$ cm^{-1} at 25 GPa makes a notable shift toward lower frequencies and becomes higher as pressure increases. It can be seen in Fig. 9(b) that at 29 GPa, a substantial amount of the spectral

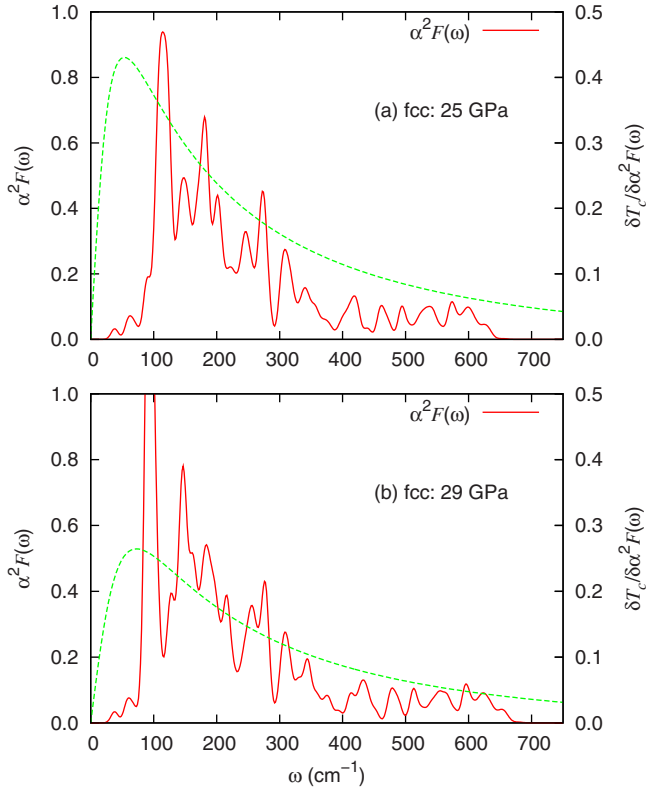

FIG. 9. (Color online) The spectral function $\alpha^2F(\omega)$ and the functional derivative $\delta T_c/\delta\alpha^2F(\omega)$ as a function of frequency ω for fcc Li for pressures (a) 25 and (b) 29 GPa. As pressure increases, a significant amount of the spectral weight is shifted toward the low-frequency region where $\delta T_c/\delta\alpha^2F(\omega)$ is largest.

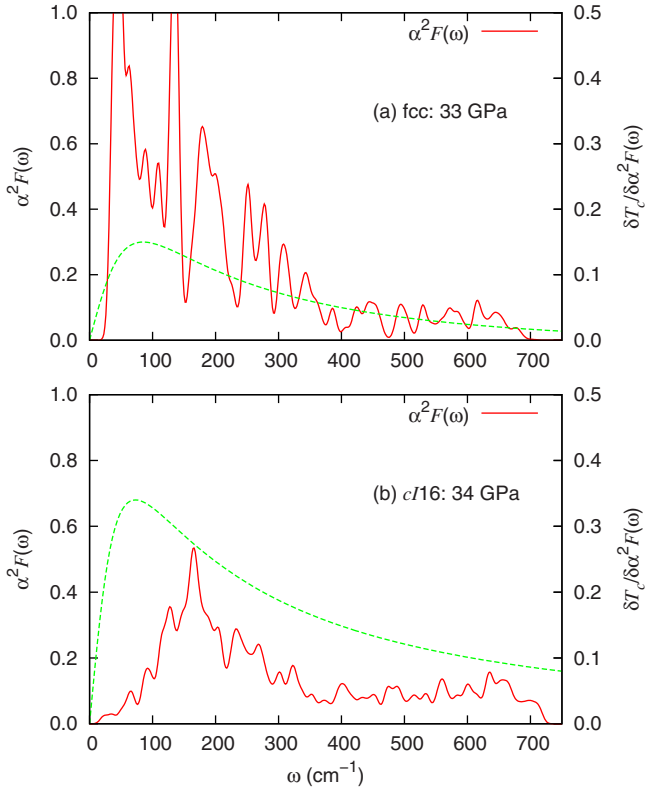

FIG. 10. (Color online) The spectral function $\alpha^2F(\omega)$ and the functional derivative $\delta T_c/\delta\alpha^2F(\omega)$ as a function of frequency ω for pressures (a) 33 GPa in the fcc phase and (b) 34 GPa in the $cI16$ phase. In the $cI16$ phase, there is little spectral weight in the frequency region where $\delta T_c/\delta\alpha^2F(\omega)$ is largest.

weight has moved to the region where $\delta T_c/\delta\alpha^2F(\omega)$ is largest, i.e., where phonons are most effective in raising T_c. At the same time, a secondary strong peak has developed at $\omega\sim 150$ cm^{-1}. As pressure is increased further, the spectral weight is concentrated more in the low-frequency region surrounding the maximum in $\delta T_c/\delta\alpha^2F(\omega)$, with the two highest peaks shifted to lower frequencies and becoming higher. This feature becomes most significant at 33 GPa, as shown in Fig. 10(a).

The value $\mu^*(\omega_{\log})=0.23$ is substantially larger than the "usual" value of $\sim 0.1-0.13$.[58] However, as mentioned above, at ambient pressure it has been estimated that $\mu^*\approx 0.24$ in the McMillan equation,[19] and the effects of Coulomb interactions are expected to be large also under pressure. If we assume the usual prescription for reducing the direct Coulomb repulsion μ to the pseudopotential μ^*, then the "maximum" value of μ^* is given by taking the limit $\mu\to\infty$ in Eq. (18) as

$$\mu^*_{\max}(\omega_{\log})\approx\frac{1}{\ln(\epsilon_F/\omega_{\log})}. \tag{20}$$

In the fcc phase, $\mu^*_{\max}\approx 0.19$ at 25 GPa and slightly decreases as pressure increases, reaching 0.17 at 33 GPa. However, the $\ln(\epsilon_F/\omega_{\log})$ reduction in Eq. (18) can easily be modified by details of Coulomb interactions.[59] The fact that the measured T_c can be reproduced with $\mu^*(\omega_{\log})=0.23$ (for

TABLE I. Eliashberg vs McMillan T_c.

Pressure (GPa)	25	26	27	28	29	30	31	32	33	34	45	57
T_c (K) Eliashberg	10.1	11.1	12.3	13.4	14.7	15.9	17.0	18.0	18.2	13.3	10.1	9.3
T_c (K) McMillan	12.1	13.1	14.2	15.3	16.4	17.4	18.1	18.4	17.1	14.3	11.4	10.7

pressure $\lesssim$29 GPa) indicates that Coulomb effects are significant in this material and cannot be fully taken into account by simply applying Eq. (18).

It is interesting to compare T_c calculated by solving the Eliashberg equations and that obtained from the Allen-Dynes modified McMillan equation[47] [Eq. (16)] as listed in Table I. Interestingly, the Eliashberg equations and the McMillan equation yield similar T_c for 9*R* and bcc Li at ambient pressure: 0.06 (0.42) K and 0.06 (0.47) K for 9*R* (bcc) for $\mu^*(\omega_{\log})=0.18$, respectively. For fcc and *cI*16, however, the approximate T_c from the McMillan equation is always higher than the T_c calculated from the Eliashberg equations (except near the fcc$\rightarrow$*cI*16 transition at 33 GPa). This may be understood due to the considerable amount of spectral weight at low frequencies, especially in the fcc phase, which results in a large EPC parameter λ given by Eq. (5) and leads to overestimation of T_c by the McMillan equation.

In Fig. 11(a) the energy gaps Δ_0 at $T=0.1T_c$ (solid lines) and T_c (dashed lines) are plotted as a function of pressure for the fcc and *cI*16 phases. The lines are guides for the eyes. The temperature $T=0.1T_c$ is low enough so that Δ_0 is the same as for zero temperature. The energy gap increases monotonously as pressure increases up to almost 4 meV at 33 GPa. In the *cI*16 phase, the gap is much smaller and has similar behavior as T_c as a function of pressure. The $2\Delta_0/k_BT_c$ as a function of pressure is shown in Fig. 11(b). The BCS value, 3.53, is indicated as a dotted line. For both fcc and *cI*16, $2\Delta_0/k_BT_c$ is larger than the BCS value, and in particular, in the fcc phase the ratio increases rapidly as pressure is increased, reaching $2\Delta_0/k_BT_c\simeq 5$ at 33 GPa and indicating strong electron-phonon coupling in this phase. In contrast, in the *cI*16 phase, the ratio stays almost constant as a function of pressure and slightly larger than the BCS value.

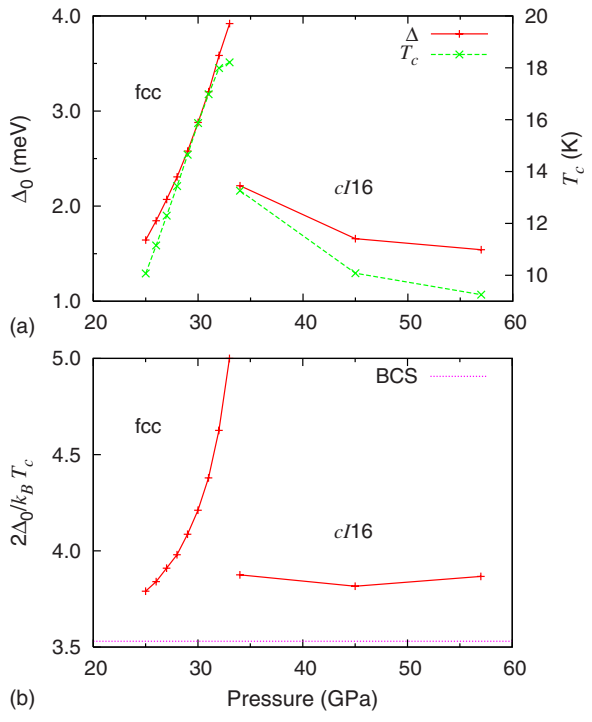

FIG. 11. (Color online) The energy gap Δ_0 along with T_c (a) and the gap ratio (b) $2\Delta_0/k_BT_c$ as a function of pressure for the fcc and *cI*16 phase. In (b) the BCS value $2\Delta_0/k_BT_c=3.53$ is indicated.

The normalized quasiparticle density of states $N(\omega)/N(0)$ given by Eq. (15) as a function of frequency is presented in Fig. 12 for 33 GPa in the fcc phase (solid curve). The BCS density of states, $\mathrm{Re}(\omega/\sqrt{\omega^2-\Delta_0^2})$, is shown as a dashed curve. The $N(\omega)$ from the Eliashberg solution exhibits a notable feature above the energy gap ($\omega\lesssim 10$ meV), deviating from the BCS density of states and indicating substantial retardation effects due to strong electron-phonon coupling.[60] This feature is most significant for fcc at 33 GPa, and it is consistent with the value of $2\Delta_0/k_BT_c$ being substantially larger than the BCS value at this pressure.

C. Superconductivity in the *cI*16 phase

The electronic band structure, phonons, and electron-phonon coupling in *cI*16 Li have been studied at three selected pressures. Pressure of 34 GPa was chosen to investigate the superconducting mechanism of *cI*16 Li close to the phase transition. A second pressure point at 45 GPa was selected to examine the pressure dependence of T_c in *cI*16 Li.

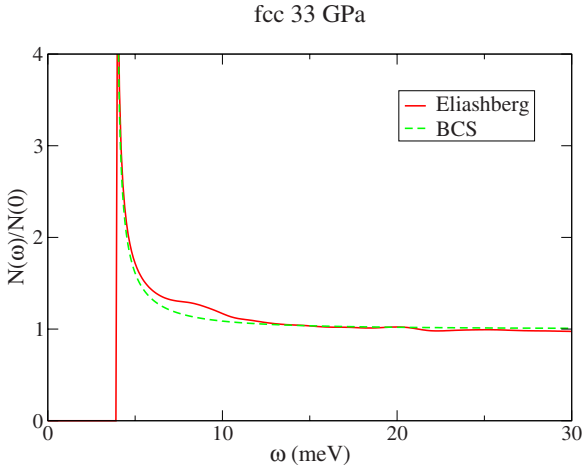

FIG. 12. (Color online) The normalized quasiparticle density of states $N(\omega)/N(0)$ as a function of frequency ω (meV) for 33 GPa in the fcc phase: the Eliashberg and BCS results are shown in solid and dashed curves, respectively.

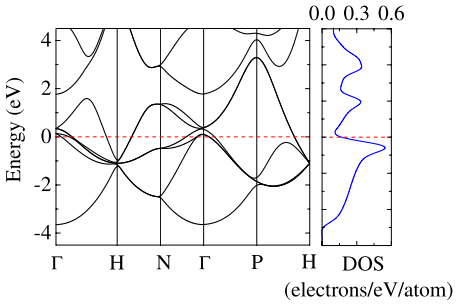

FIG. 13. (Color online) The electronic band structure and DOS of *cI*16 Li at 34 GPa.

Higher pressure of 57 GPa was chosen to explore the structural stability of *cI*16 Li since a structural phase transition was suggested by the Raman spectroscopy data[10] near 50 GPa. The electronic band structure and DOS were computed with a $32\times32\times32$ MP k-point mesh. Individual phonon calculations were performed on an $8\times8\times8$ MP q-point mesh with a $16\times16\times16$ MP k-point mesh for the first BZ integrations. The EPC parameter λ_{qj} has been computed in the first BZ on an $8\times8\times8$ MP q-point mesh using individual EPC matrices obtained with a $32\times32\times32$ k-point mesh.

The electronic band structure and DOS of *cI*16 Li at 34 GPa are shown in Fig. 13. The calculated DOS agrees with that from a previous study.[9] A peak appears near the top of the occupied states in the DOS, with the Fermi level located in a valley. Compared with the smooth decrease in the DOS near the Fermi level in fcc and *hR*1 Li (not shown), the substantially lower electronic density of states at the Fermi level in *cI*16 Li indicates a tendency toward opening of a band gap. The electronic bands crossing the Fermi level are very dispersive except around Γ. This feature is in contrast to fcc Li, in which the electronic bands are flat and almost parallel to the Fermi level near the L point.[32,35,36] Thus the spherical FS in fcc Li is distorted anisotropically and has parallel necks at the boundary of the first BZ. The Fermi-surface nesting between these necks has been shown to be the origin of strong EPC in fcc Li.[31,32]

The phonon band structures of *cI*16 Li at 34, 45, and 57 GPa are depicted in Fig. 14 (for clarity only the acoustic branches are shown for the latter two pressures). The phonon band structure exhibits no imaginary modes, indicating that *cI*16 Li is dynamically stable up to at least 57 GPa. The most significant feature of the phonon band structure is that the vibrational modes near H are softened as pressure increases. In previous studies of fcc Li, the phonon softening was suggested to be induced by a change in the electronic structure near the Fermi surface that can be examined in terms of the nesting function,[30,61]

$$\xi(q) = \frac{1}{N}\sum_{nm}\sum_{k}\delta(\epsilon_{kn}-\epsilon_F)\delta(\epsilon_{k+qm}-\epsilon_F)$$

$$\propto \sum_{nm}\oint dl_k \frac{1}{|\vec{v}_{kn}\times\vec{v}_{k+qm}|}, \qquad (21)$$

where N is the number of k points. The ϵ_{kn} and ϵ_{k+qm} are the

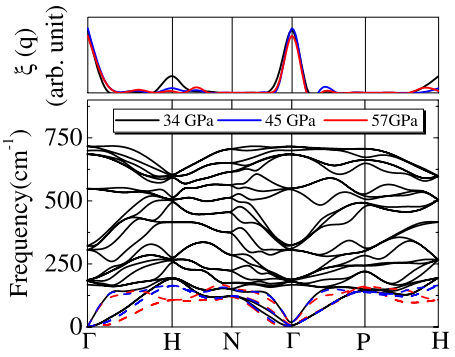

FIG. 14. (Color online) The phonon band structure (bottom) and nesting functions $\xi(q)$ (top) for *cI*16 Li calculated at 34, 45, and 57 GPa. Only acoustic modes are shown in the phonon band structure for the latter two pressures.

Kohn-Sham eigenvalues with wave vectors k and $k+q$ within the nth and mth bands, respectively. The $\vec{v}_{kn}$ and $\vec{v}_{k+qm}$ are the Fermi velocities. The line integral is along the intersection of the Fermi surface and its image displaced by vector q. The $\xi(q)$ represents an approximation of the phonon linewidth in Eq. (3) assuming that the strength of EPC is constant in the first BZ and over all phonon modes j, i.e., $g^j_{kn,k+qm}=1$. The calculated $\xi(q)$ of *cI*16 Li at 34, 45, and 57 GPa are shown in Fig. 14 (top). The large peaks around the Γ point reflect the nesting of the entire FS with itself and thus have no physical meaning. The most significant nesting occurs near the H point. However, the strength of the nesting decreases with pressure due to phonon softening. Halfway through the $\Gamma\rightarrow H$, $H\rightarrow N$, and $\Gamma\rightarrow P$ directions, there are small FS nestings that are also associated with phonon softenings. The results show that FS nesting in *cI*16 Li is much weaker and more localized than that in the fcc phase. In the latter case, FS nesting was found to be very large along the $\Gamma\rightarrow X$ direction.[30] It can be seen in Eq. (4) that FS nesting and the electron-phonon matrix elements are the two main factors dictating the EPC strength. The EPC parameter λ is determined by a balance between $\xi(q)$ and $g^j_{kn,k+qm}$ and is analyzed and discussed below.

The λ and $\omega_{\log}$ at 34 GPa are 0.98 and 233 K, respectively. These values are to be compared with the very large $\lambda=3.14$ for fcc Li at 33 GPa. The substantially reduced λ is particularly interesting. The spectral function $\alpha^2F(\omega)$ for *cI*16 Li at 34 GPa and the integrated EPC parameter λ as a function of frequency ω are shown in Fig. 15 (top). The $\alpha^2F(\omega)$ exhibits gross similarity with the PHDOS [Fig. 15 (bottom)]. As observed from the integrated λ, major contributions to EPC are from the broad peak below 250 cm^{-1}. Incidentally, ω for which the spectral function has its maximum coincides with $\omega_{\log}$. The λ and $\omega_{\log}$ both decrease slowly with pressure and reach 0.92 and 211 K at 45 GPa. At 57 GPa, λ increases to 0.96, while $\omega_{\log}$ continues to decrease down to 180 K. The decrease in λ between 34 and 45 GPa is consistent with the reduction in overall FS nesting shown in Fig. 14. This indicates that the electron-phonon matrix elements $g^j_{kn,k+qm}$ do not vary appreciably in this pressure range. On the other hand, from 45 to 57 GPa, the modest increase in λ indicates that the $g^j_{kn,k+qm}$ are enhanced.

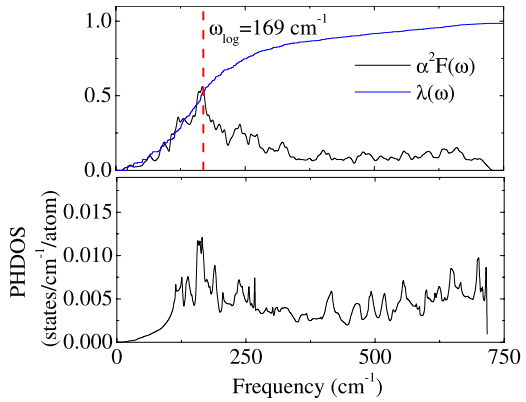

FIG. 15. (Color online) The spectral function $\alpha^2F(\omega)$ and integrated EPC parameter λ (top) and the phonon density of states (bottom) as a function of frequency ω in the $cI16$ phase at 34 GPa.

The T_c obtained by solving the Eliashberg equations for 34, 45, and 57 GPa are shown in Fig. 7, which reproduces the experimental values very well with $\mu^*(\omega_{\log})=0.12$. It is interesting that in the $cI16$ phase μ^* is much smaller than in the fcc phase at lower pressure and the $9R$ phase at ambient pressure and within the range of the usual value of $\sim 0.1-0.13$.[58] The change in T_c from 34 to 45 GPa can be traced back to simultaneous decrease in the Debye temperature and the density of electronic states at the Fermi level. The drastic reduction in T_c from 33 (fcc) to 34 GPa ($cI16$) can be understood by comparing $\alpha^2F(\omega)$ and $\delta T_c/\delta\alpha^2F(\omega)$ as a function of ω, as shown in Fig. 10. In contrast to fcc Li at 33 GPa [Fig. 10(a)], in the $cI16$ phase at 34 GPa [Fig. 10(b)], there is little spectral weight in the low-frequency region where $\delta T_c/\delta\alpha^2F(\omega)$ is largest, and the phonons with higher frequencies are not very effective in raising T_c. This explains the sharp drop of T_c from 18 K at 33 GPa to 13 K at 34 GPa. The structural stability established by phonons and the reasonable value of the predicted T_c hints that $cI16$ Li may exist or coexist with other structures in this pressure range.

IV. SUMMARY

The electronic structure, phonons, and superconducting properties of three superconducting phases ($9R$, fcc, and $cI16$) of solid Li have been studied by means of first-principles calculations. Within the quasiharmonic approximation, it has been found that the bcc$\rightarrow 9R$ transformation occurs at $T=220$ K at ambient pressure. From the Eliashberg theory, the superconducting critical temperature T_c in bcc and $9R$ Li has been estimated. The observed T_c can be reproduced if the Coulomb pseudopotential $\mu^*\approx 0.23$ is used in the McMillan equation for $9R$ Li. The T_c for bcc Li is substantially higher than the experimental value with a reasonable choice of μ^*. This observation supports the suggestion that $9R$ is the superconducting phase found in the recent experiment.[25]

The pressure-induced phase transition fcc$\rightarrow cI16$ has been investigated. The nature of superconductivity in both phases has been examined by directly solving the Eliashberg equations with the spectral function $\alpha^2F(\omega)$ obtained from first-principles calculations and by evaluating the functional derivative $\delta T_c/\delta\alpha^2F(\omega)$. The fcc$\rightarrow cI16$ transition pressure of 33 GPa determined from the calculated enthalpies is close to the pressure where phonon softening is found. The estimated T_c in the fcc phase for pressure 25–33 GPa increases with pressure until the transition to $cI16$ Li occurs. The predicted T_c for fcc Li is in good agreement with the experimental data[13–15] except for close to the structural transition point, where anharmonicity may play a dominant role. As pressure is increased from 25 GPa, the spectral weight is shifted toward the low-frequency region, where $\delta T_c/\delta\alpha^2F(\omega)$ is largest and phonons are most effective in raising T_c. This feature is found to be most significant at 33 GPa, where T_c reaches a maximum consistently with the trend found in the experiment in Ref. 14. To reproduce the experimental T_c (for pressure not too close to the transition point), $\mu^*(\omega_{\log})=0.23$ was needed. This indicates that as in the $9R$ phase at ambient pressure, the effects of Coulomb interactions are significant in this low-density metal.

The $cI16$ phase has been studied at three pressures: 34, 45, and 57 GPa. It is found that $cI16$ Li is stable within this pressure range. From the solution of the Eliashberg equations, T_c that agrees very well with the experimental value has been obtained with $\mu^*(\omega_{\log})=0.12$. There is a sudden drop of T_c after the fcc$\rightarrow cI16$ transition, which is due to a significant reduction in the spectral weight in the low-frequency region where $\delta T_c/\delta\alpha^2F(\omega)$ is largest. The structural stability and the reasonable predicted T_c at 57 GPa indicate the possibility that $cI16$ Li is stable beyond 50 GPa.

ACKNOWLEDGMENTS

One of the authors (K.T.) would like to thank J. P. Carbotte and E. J. Nicol for helpful discussions. The research was supported by the Natural Sciences and Engineering Research Council of Canada and the Canada Foundation for Innovation.

*Corresponding author: John.Tse@usask.ca
†Corresponding author: kat221@mail.usask.ca

[1] R. Rousseau and D. Marx, Chem.-Eur. J. **6**, 2982 (2000).
[2] C. S. Barrett, Acta Crystallogr. **9**, 671 (1956).
[3] A. W. Overhauser, Phys. Rev. Lett. **53**, 64 (1984).
[4] H. G. Smith, Phys. Rev. Lett. **58**, 1228 (1987).
[5] W. Schwarz and O. Blaschko, Phys. Rev. Lett. **65**, 3144 (1990).
[6] B. Olinger and W. Shaner, Science **219**, 1071 (1983).
[7] M. Hanfland, I. Loa, K. Syassen, U. Schwarz, and K. Takemura, Solid State Commun. **112**, 123 (1999).

[8] V. V. Struzhkin, R. J. Hemley, and H. K. Mao, Bull. Am. Phys. Soc. **44**, 1489 (1999).
[9] M. Hanfland, K. Syassen, N. E. Christensen, and D. L. Novikov, Nature (London) **408**, 174 (2000).
[10] A. F. Goncharov, V. V. Struzhkin, H. K. Mao, and R. J. Hemley, Phys. Rev. B **71**, 184114 (2005).
[11] R. Rousseau, K. Uehara, D. D. Klug, and J. S. Tse, ChemPhysChem **6**, 1703 (2005); Y. Ma, A. R. Oganov, and Y. Xie, Phys. Rev. B **78**, 014102 (2008).
[12] T. H. Lin and K. J. Dunn, Phys. Rev. B **33**, 807 (1986).
[13] K. Shimizu, H. Ishikawa, D. Takao, T. Yagi, and K. Amaya, Nature (London) **419**, 597 (2002).
[14] V. V. Struzhkin, M. I. Eremets, W. Gan, H.-K. Mao, and R. J. Hemley, Science **298**, 1213 (2002).
[15] S. Deemyad and J. S. Schilling, Phys. Rev. Lett. **91**, 167001 (2003).
[16] D. A. Papaconstantopoulos, L. L. Boyer, B. M. Klein, A. R. Williams, V. L. Morruzzi, and J. F. Janak, Phys. Rev. B **15**, 4221 (1977).
[17] A. Y. Liu and M. L. Cohen, Phys. Rev. B **44**, 9678 (1991).
[18] A. Y. Liu and A. A. Quong, Phys. Rev. B **53**, R7575 (1996).
[19] C. F. Richardson and N. W. Ashcroft, Phys. Rev. B **55**, 15130 (1997).
[20] A. Y. Liu, A. A. Quong, J. K. Freericks, E. J. Nicol, and E. C. Jones, Phys. Rev. B **59**, 4028 (1999).
[21] J. K. Freericks, S. P. Rudin, and A. Y. Liu, Physica B **284-288**, 425 (2000).
[22] A. Y. Liu, Phys. Status Solidi B **217**, 419 (2000).
[23] T. L. Thorp, B. B. Tripplett, W. D. Brewer, M. L. Cohen, N. E. Phillips, D. A. Shirley, J. E. Templeton, R. W. Stark, and P. H. Schmidt, J. Low Temp. Phys. **3**, 589 (1970).
[24] K. M. Lang, A. Mizel, J. Mortara, E. Hudson, J. Hone, M. L. Cohen, A. Zettl, and J. C. Davis, J. Low Temp. Phys. **114**, 445 (1999).
[25] J. Tuoriniemi, K. Juntunen-Nurmilaukas, J. Uusvuori, E. Pentti, A. Salmela, and A. Sebedash, Nature (London) **447**, 187 (2007).
[26] N. E. Christensen and D. L. Novikov, Phys. Rev. Lett. **86**, 1861 (2001).
[27] A. Razzaque, A. K. M. A. Islam, F. N. Islam, and M. N. Islam, Solid State Commun. **131**, 671 (2004).
[28] J. S. Tse, Y. Ma, and H. M. Tutuncu, J. Phys.: Condens. Matter **17**, S911 (2005).
[29] S. U. Maheswari, H. Nagara, K. Kusakabe, and N. Suzuki, J. Phys. Soc. Jpn. **74**, 3227 (2005).
[30] D. Kasinathan, J. Kunes, A. Lazicki, H. Rosner, C. S. Yoo, R. T. Scalettar, and W. E. Pickett, Phys. Rev. Lett. **96**, 047004 (2006).
[31] G. Profeta, C. Franchini, N. N. Lathiotakis, A. Floris, A. Sanna, M. A. L. Marques, M. Lüders, S. Massidda, E. K. U. Gross, and A. Continenza, Phys. Rev. Lett. **96**, 047003 (2006).
[32] K. Iyakutti and C. N. Louis, Phys. Rev. B **70**, 132504 (2004).
[33] L. Shi and D. A. Papaconstantopoulos, Phys. Rev. B **73**, 184516 (2006).
[34] N. E. Christensen and D. L. Novikov, Phys. Rev. B **73**, 224508 (2006).
[35] A. Rodriguez-Prieto, A. Bergara, V. M. Silkin, and P. M. Echenique, Phys. Rev. B **74**, 172104 (2006).
[36] Y. Xie, J. S. Tse, T. Cui, A. R. Oganov, Z. He, Y. Ma, and G. Zou, Phys. Rev. B **75**, 064102 (2007).
[37] R. A. Jishi, M. Benkraouda, and J. Bragin, J. Low Temp. Phys. **147**, 549 (2007).
[38] G. M. Eliashberg, Zh. Eksp. Teor. Fiz. **38**, 966 (1960) [Sov. Phys. JETP **11**, 696 (1960)].
[39] S. Baroni, P. Giannozzi, and A. Testa, Phys. Rev. Lett. **58**, 1861 (1987).
[40] P. Giannozzi, S. de Gironcoli, P. Pavone, and S. Baroni, Phys. Rev. B **43**, 7231 (1991).
[41] S. Baroni, S. de Gironcoli, A. Dal Corso, and P. Giannozzi, Rev. Mod. Phys. **73**, 515 (2001); P. Giannozzi *et al.*, http://www.quantum-espresso.org
[42] J. P. Carbotte, Rev. Mod. Phys. **62**, 1027 (1990); F. Marsiglio and J. P. Carbotte, in *Superconductivity: Conventional and Unconventional Superconductors*, edited by K. H. Bennemann and J. B. Ketterson (Springer-Verlag, Berlin, 2008), pp. 73–162.
[43] G. Bergmann and D. Rainer, Z. Phys. **263**, 59 (1973).
[44] P. B. Allen and R. C. Dynes, Phys. Rev. B **12**, 905 (1975).
[45] F. Marsiglio, M. Schossmann, and J. P. Carbotte, Phys. Rev. B **37**, 4965 (1988).
[46] W. L. McMillan, Phys. Rev. **167**, 331 (1968).
[47] P. B. Allen and R. C. Dynes, J. Phys. C **8**, L158 (1975).
[48] N. N. Bogoliubov, N. V. Tolmachev, and D. V. Shirkov, *A New Method in the Theory of Superconductivity* (Consultants Bureau, New York, 1959).
[49] P. Morel and P. W. Anderson, Phys. Rev. **125**, 1263 (1962).
[50] H. J. Monkhorst and J. D. Park, Phys. Rev. B **13**, 5188 (1976).
[51] A. H. MacDonald, S. H. Vosko, and P. T. Coleridge, J. Phys. C **12**, 2991 (1979).
[52] J. B. Neaton and N. W. Ashcroft, Nature (London) **400**, 141 (1999).
[53] G. Kresse and J. Furthmüller, Comput. Mater. Sci. **6**, 15 (1996).
[54] G. Kresse and D. Joubert, Phys. Rev. B **59**, 1758 (1999).
[55] H. J. Choi, D. Roundy, H. Sun, M. L. Cohen, and S. G. Louie, Phys. Rev. B **66**, 020513(R) (2002).
[56] A. Mialitsin, B. S. Dennis, N. D. Zhigadlo, J. Karpinski, and G. Blumberg, Phys. Rev. B **75**, 020509(R) (2007).
[57] B. Mitrović and J. P. Carbotte, Solid State Commun. **37**, 1009 (1981).
[58] Y. G. Jin and K. J. Chang, Phys. Rev. B **57**, 14684 (1998).
[59] F. Marsiglio, Physica C **160**, 305 (1989); J. Low Temp. Phys. **87**, 659 (1992).
[60] W. L. McMillan and J. M. Rowell, in *Superconductivity*, edited by R. D. Parks (Dekker, New York, 1969), p. 561.
[61] M. Wierzbowska, S. de Gironcoli, and P. Giannozzi, arXiv:cond-mat/0504077 (unpublished).